Fabrication process for 200 nm-pitch polished freestanding ultrahigh aspect ratio gratings

Alexander R. Bruccoleri[a)]
Izentis LLC, P.O. Box 397002, Cambridge, Massachusetts 02139-7002

Ralf K. Heilmann and Mark L. Schattenburg
Space Nanotechnology Laboratory, MIT Kavli Institute for Astrophysics and Space Research, Massachusetts Institute of Technology, Cambridge, Massachusetts 02139

(Received 24 June 2016; accepted 18 October 2016; published 2 November 2016)

A fully integrated fabrication process has been developed to fabricate freestanding, ultrahigh aspect ratio silicon gratings with potassium hydroxide (KOH)-polished sidewalls. The gratings are being developed for wavelength-dispersive, soft x-ray spectroscopy on future space telescopes. For this application, the grating needs to have a large open-area fraction and smooth sidewalls (roughness < 1 nm) to maximize efficiency. The prototype gratings fabricated with the process presented here have been tested on a synchrotron beamline and have demonstrated an absolute diffraction efficiency greater than 30% for 2 nm-wavelength x-rays in blazed orders. This efficiency is greater than twice the efficiency of previously fabricated gratings. The fabrication process utilizes silicon-on-insulator wafers where the grating and a cross support are etched in the device layer, and an additional structural support is etched in the handle layer. The device layer and handle layer are both etched via deep reactive-ion etching using a Bosch process. The buried SiO_2 layer stops both etches and is removed at the end of the process to create a freestanding structure. The gratings have a pitch of 200 nm, a depth of 4 μm, and the bars are polished via KOH. The polishing process reduces both the roughness and the grating-bar thickness. The finished gratings span an area of approximately 10 by 30 mm, supported by 1 mm-wide hexagons in the handle layer. © *2016 American Vacuum Society*.
[http://dx.doi.org/10.1116/1.4966595]

I. INTRODUCTION

This paper presents a fabrication process for freestanding, ultrahigh aspect ratio silicon gratings with potassium hydroxide (KOH)-polished sidewalls. The primary application of this fabrication process is the critical-angle transmission (CAT) grating. As described in previous works,[1,2] the CAT grating is a blazed transmission grating intended to be a component for a wavelength-dispersive, soft x-ray spectrometer onboard space telescopes.[3–5] Specifically, there is interest in the x-ray band with energies below 1 keV that covers the emission lines of carbon, nitrogen, oxygen, neon, and iron.[6,7] There are also many other applications for similar freestanding structures, including neutral mass spectroscopy,[8] ultraviolet filtration,[9] and phase contrast imaging.[10]

The past work demonstrated a process for freestanding ultrahigh aspect ratio silicon gratings[1] as well as a process to polish grating sidewalls via KOH.[11] The integration of these two processes required new developments to eliminate defects, which are the focus of this paper. Specifically, three new process improvements were developed: (1) An improved deep reactive-ion etch (DRIE) Bosch process was developed for etching 200 nm-pitch grating bars. This etch enabled damage-free lines post KOH polishing. KOH polishing is necessary to reduce the roughness of the sidewalls from $\sim$4 nm root mean square after the Bosch process, to $\lesssim$1 nm for efficient reflection of soft x-rays. KOH polishing also thins the grating bars increasing the open-area fraction, further increasing the diffraction efficiency. (2) A novel procedure was developed to fill and protect the CAT grating lines post KOH polishing, enabling damage-free membranes. (3) A gentle vapor hydrofluoric acid (HF) process was also developed to remove buried SiO_2, which yielded virtually damage-free, freestanding gratings.

Space telescopes often observe faint objects, and diffraction efficiency is a critical mission parameter.[12–14] There is also a desire for improved resolution, which further increases the requirements for efficiency.[15] The CAT grating efficiently utilizes incident x-rays by reflecting them from the grating sidewalls at a graze angle θ_i, which is near or below the critical angle for total external reflection, θ_c (see Fig. 1). Diffraction occurs when the optical path length difference (OPLD) between parallel x-rays offset by one grating period is an integer multiple of the x-ray wavelength. Precisely, for specular reflection the OPLD for diffraction equals $2P\sin(\theta_i) = m\lambda$, and the general grating equation is

$$m\lambda = P(\sin(\theta_i) + \sin(\beta_m)), \tag{1}$$

where m is the diffraction order, λ is the wavelength, P is the grating period, θ_i is the angle of incidence, and β_m is the angle of the outgoing diffraction orders. The CAT grating geometry results in the outgoing x-rays being channeled into the nonzero diffraction orders, such that θ_i and β_m are similar in value. Ideally, the diffraction orders are centered around the angle of specular reflection. This blazing effect increases efficiency over traditional transmission gratings where most of the outgoing light is in the zeroth and $\pm$ first diffraction

a)Electronic mail: alex@izentis.com

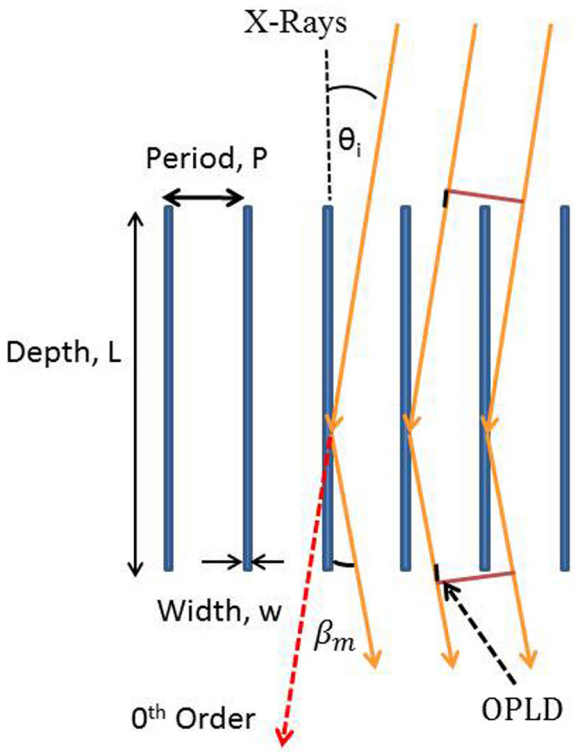

FIG. 1. (Color online) Conceptual geometric drawing of CAT grating cross section (not to scale).

orders. Utilizing higher diffraction orders also increases the spectral resolving power.

Previously, state-of-the-art space-based x-ray transmission gratings, developed and launched on the Chandra x-ray observatory, were made of phase-shifting gold bars on a membrane.[16] The gold and the membrane absorbed soft x-rays and therefore was ineffective below 1 keV.[17–19] See Fig. 2 for a plot of absolute diffraction efficiency of CAT gratings versus wavelength. The measurements were taken at the Advanced Light Source, Lawrence Berkeley National Laboratory, with CAT gratings fabricated with the process presented here. These tests showed record broadband-diffraction efficiency in the soft x-ray band, which will enable significant advances in x-ray astronomy. Furthermore, these gratings have undergone resolving power tests with x-ray mirrors at NASA Marshall Space Flight Center. Preliminary results indicate resolutions ($\lambda/\Delta\lambda$) in excess of 10 000 for the aluminum $K_{\alpha 1,2}$ lines.[20]

II. FABRICATION METHODOLOGY

The CAT grating is fabricated as a monolithic structure from a silicon-on-insulator (SOI) wafer. The SOI wafer is made up of a 4 μm-thick $\langle 110 \rangle$ device layer, a 500 nm-thick buried SiO_2, and a 500 μm-thick $\langle 100 \rangle$ handle layer. Past works have demonstrated key steps such as ultrahigh aspect ratio DRIE, integration of two DRIE steps to make freestanding, unpolished gratings, and polishing gratings in bulk silicon.[1,11] Significant advancements have been made to enable an integrated process with polished grating bars, and minimal damage to both the grating membranes and individual grating bars. The handle layer is etched via a standard

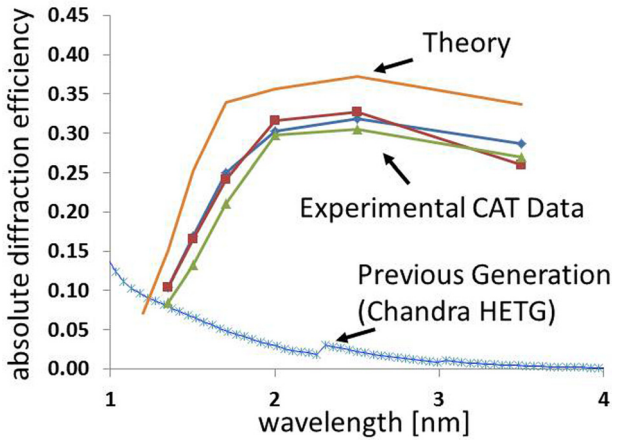

FIG. 2. (Color online) Plot of absolute diffraction efficiency vs wavelength for CAT gratings and the Chandra high-energy transmission gratings (Ref. 5). Different geometries are predicted to lead to efficiencies >50% (Ref. 14).

Bosch DRIE process into hexagons spanning roughly 1 mm, which are designated the level 2 supports. Both DRIE steps stop on the same buried SiO_2, which is removed at the end to create a freestanding structure. Arrays of hexagons make up the structure that spans roughly 10 × 30 mm, which can be bonded to metal or composite frames and tiled together to create the final grating array for a telescope. See Fig. 3 for a conceptual drawing of a single hexagon cell.

Figure 4 depicts the CAT grating process flow. The initial step is to mask and etch the hexagonal level 2 support structure mask in the back side, PECVD SiO_2, via contact lithography and inductively coupled plasma (ICP) reactive-ion etching. The {111} planes are located via a wagon-wheel and KOH pre-etch.[11,21] This step is critical as the {111} planes act as an etch stop for KOH and must be aligned to the CAT grating bars within ±0.2°.

The level 1 supports are patterned via interference lithography in a 30 nm-thick chrome layer on top of the 300 nm-thick layer of thermal SiO_2. The 200 nm-pitch CAT grating lines are patterned parallel to the {111} planes on a trilayer

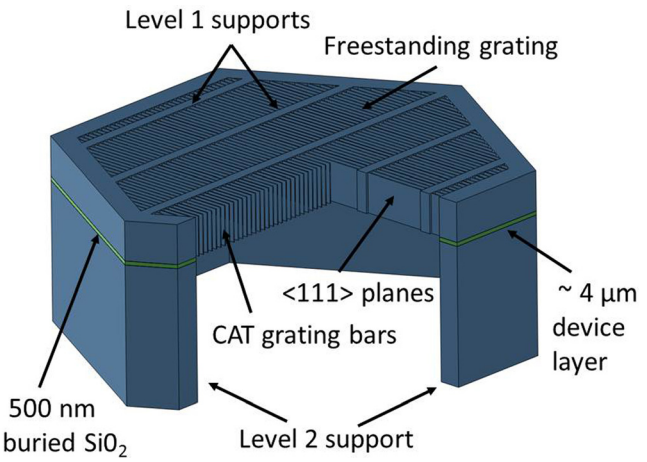

FIG. 3. (Color online) CAD depiction of one CAT grating membrane cell with structural supports. The CAT grating and a 5 μm-pitch cross support structure (level 1 supports) are etched in the device layer (not to scale).

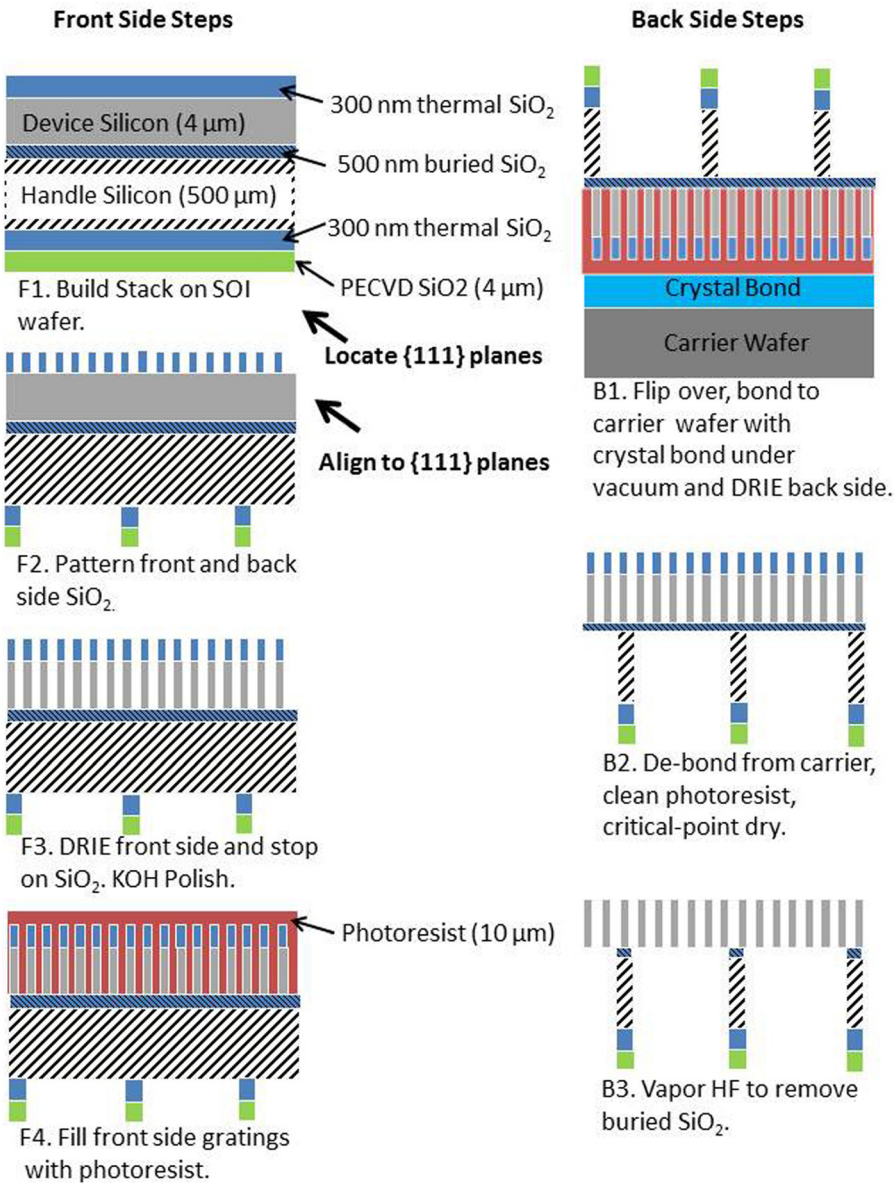

FIG. 4. (Color online) Process flow for CAT grating fabrication.

stack, which is put down over the thermal SiO_2 and prepatterned chrome lines. The trilayer stack is then etched into the thermal SiO_2 to create a two-dimensional hard mask with the CAT grating and level 1 support lines.[22,23]

The 2D thermal SiO_2 mask is used for the CAT grating DRIE via an SPTS Pegasus etch tool. The details of the DRIE step are critical to obtaining an undamaged CAT grating structure and are presented in Sec. III. After DRIE, the grating is cleaned in a mixture of H_2SO_4 and H_2O_2 (piranha) to remove polymer. Any residual chrome is removed via 120 s etch in CR-7. The native SiO_2 on the grating sidewalls is removed via 50:1 diluted HF for 60 s to avoid damaging the mask or buried SiO_2. Following the cleaning steps, the grating is polished for 2 min in a 50% (by weight) solution of KOH at room temperature, with 0.02% surfactant, sodium dihexyl sulfosuccinate. Various polishing concentrations from 10% to 50% and times from 30 s to 40 min were experimented with, and 2 min at 50% achieved good x-ray efficiency results without damage.[5]

After KOH polishing, the CAT grating channels are filled and protected with photoresist, with details provided in Sec. IV. The protected CAT grating is bonded to a carrier wafer via Crystalbond 555 on a hotplate at 90 °C in a vacuum chamber. The back-side mask is manually cleaned via isopropyl alcohol on wipes. The back side is etched via a Bosch process and carefully monitored with a camera to stop on the buried SiO_2 without over-etching. Approximately 150 nm of the buried SiO_2 is etched from the back via RIE with H_2 and CF_4. This is done to make the buried SiO_2 removal step easier at the end of the process. To remove the sample from the carrier, it is immersed in roughly 500 ml water and put on a hotplate set to 220 °C until the Crystalbond melts, and the sample gently floats off the carrier. After separation, the sample is piranha cleaned twice and critical-point dried. The

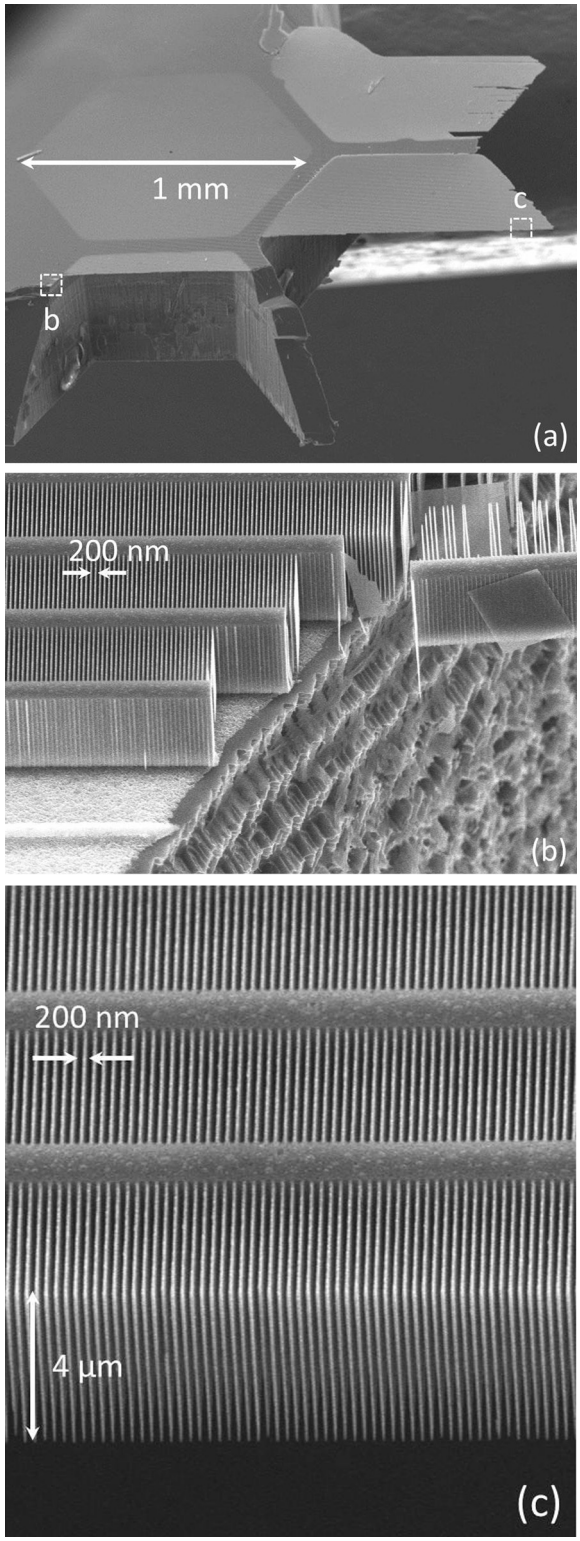

FIG. 5. (a) Zoomed-out SEM imagery of a cleaved 200 nm-pitch freestanding CAT grating. (b) Cross section SEM imagery of CAT grating lines on a level 2 support structure. The scallops from the back-side etch are clearly observed. (c) Cross section SEM imagery of freestanding CAT grating.

buried SiO_2 is finally removed slowly via vapor HF to create a freestanding structure. See Fig. 5 for SEM images of a cleaved freestanding grating. These images provide a sense of scale to the CAT grating. The zoomed-out image clearly shows the hexagonal, level 2 support. The CAT grating and level 1 supports are seen as a membrane when zoomed out. Figure 5(b) shows the region where the CAT grating and back-side etch meet on the edge of a hexagon. Figure 5(c) zooms-in on the freestanding CAT grating bars and level 1 support structure. Two oblique SEM images of another freestanding CAT grating are shown in Fig. 6.

III. NANOSCALE HIGH-ASPECT RATIO BOSCH PROCESS

The DRIE step on the 200 nm-pitch CAT grating determines the profile and ultimately the quality of the grating bars. Past developments with KOH polishing showed the widths of the grating bars at the top would etch faster than at the base. From past SEM inspection, the tops would etch approximately twice as fast, ≈2 vs 1 nm/min. The desired profile of the finished CAT grating is vertical to maximize the open-area fraction. As a result, the ideal profile after DRIE would have a reverse-tapered profile with the grating bars gradually thinning at the base. Past DRIE tests also had either bowed profiles such that the middle of the grating bar was the thinnest, or positively tapered such that the bottoms of the bars were thickest.[11,23,24] Both of these profiles would not yield large open-area fractions with KOH polishing. In order to control the etch profile, a series of experiments were conducted to gain a qualitative understanding of DRIE for nanoscale, ultrahigh aspect ratio structures.

The Bosch process was used for all experiments, which is a two-step process depicted in Fig. 7.[25] The steps are

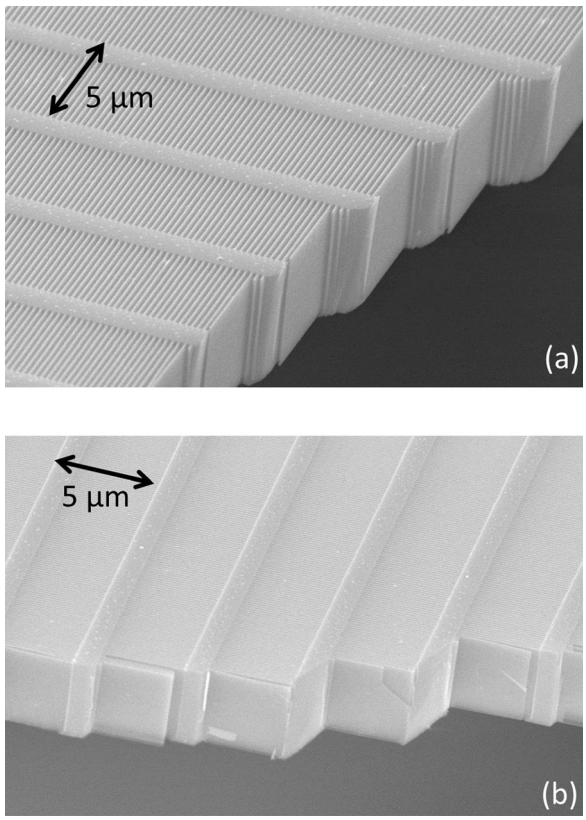

FIG. 6. SEM images of a cleaved high quality 200 nm-pitch freestanding CAT grating membrane.

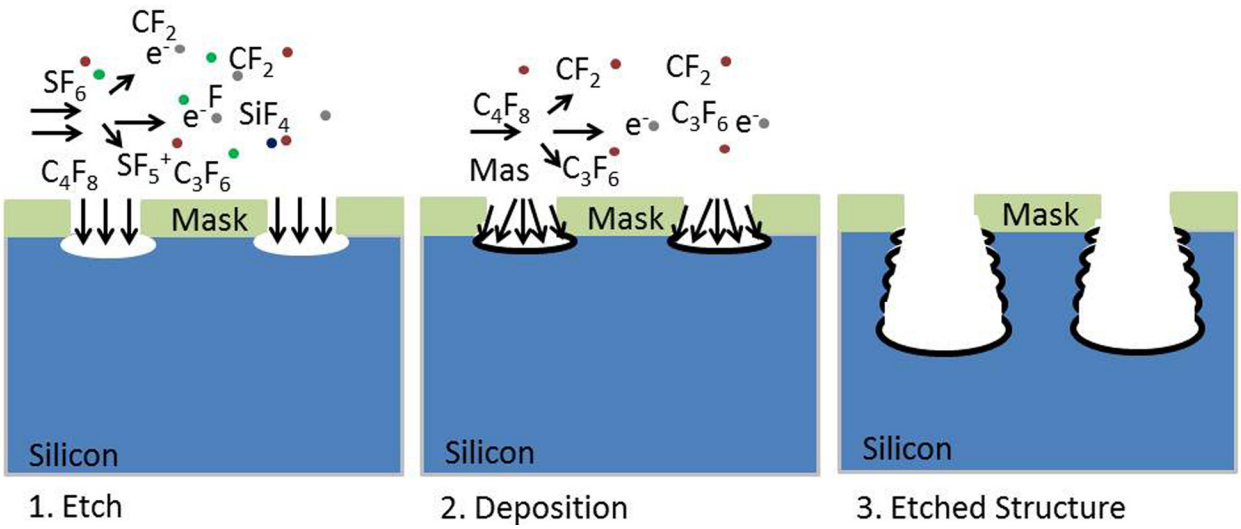

FIG. 7. (Color online) Conceptual drawing of Bosch process with tapered profile.

designated "etch" and "deposition." Traditionally, the etch step utilizes SF_6 and the deposition step C_4F_8. Both steps ionize the gas in an ICP source, and only the etch step applies a bias voltage to the sample. During the etch step, the free radicals of fluorine etch the silicon isotropically; however, this step is only on the order of seconds. The deposition step isotropically coats the sample with a fluorocarbon polymer and is of similar duration. The subsequent etch step removes the polymer at the base of the trenches due to the high vertical flux and momentum of the ions; however, the sidewall polymer remains relatively intact due to minimal lateral motion. The exposed silicon can then be etched isotropically by the neutral fluorine, and the process repeats creating an anisotropic etch.

The basic Bosch process has been modified for numerous applications, and modern DRIE tools allow for ramping of the parameters. This means that the power, mass flows, durations, etc., can vary linearly with time with each step. As a result, the profile of the grating bars can be controlled with time. The initial etch process presented in Ref. 11 is shown in Table I. The etch step uses C_4F_8, which adds polymer growth, and reduces the lateral etch of the neutral fluorine. The C_4F_8 flow rate in the etch step was ramped from 50 to 25 SCCM. The platen power also ramped from 50 to 65 W, which therefore ramped the bias voltage to the sample.

TABLE I. Original nanoscale DRIE parameters.

Device parameter	Deposition cycle	Etch cycle
SF_6 flow rate (SCCM)	0	175
C_4F_8 flow rate (SCCM)	150	50–25
Coil power (W)	1500	1500
Platen power (W)	0	50–65
Cycle time (s)	1.5	1.5
Base pressure (mTorr)	10	10
Chuck temperature (°C)	−15	−15
Etch duration	190 loops	

The tapered profile generated by the baseline recipe was altered to produce reverse tapered profiles, which after KOH polishing produces the desired straighter profiles. To do so, both gas flow ramp rates and step duration times were altered. The grating bars can be made thinner by increasing the duration and potency (increased SF_6 partial pressure, coil power, etc.), of the etch step with time, or by decreasing the duration of the deposition step. A reverse taper on nanoscale lines was demonstrated by Mirza *et al.* by also adjusting the ratio of SF_6/C_4F_8 in a continuous etch via an ICP source.[26] See Fig. 7, step 3, for a conceptual drawing of a Bosch process with a tapered profile. The first etch profiles with reverse tapers were achieved by changing the C_4F_8 flow-ramp from 50–25 SCCM to a ramp of 25–0 SCCM. This change led to a significant taper, and the bars were less than 50 nm-thick at the base. The subsequent KOH polishing step resulted in an approximately vertical profile; however, the lines were under 50 nm thick and showed damage in some regions. See Fig. 8 for SEM images of the tapered DRIE and subsequent KOH polish.

To reduce the taper the C_4F_8 flow-ramp was adjusted from 25–0 SCCM to 25–10 SCCM. SEM images of the cross section are shown in Fig. 9. This resulted in grating bars roughly 70 nm-thick at the base, and this same sample leads to a high quality freestanding grating shown in Fig. 5.

Further experiments were developed to create a thicker profile to allow for longer KOH polishing times at higher concentrations. A nearly vertical etch was developed by ramping the etch step from 1.2 to 1.5 s and the deposition step from 1.5 to 1.2 s while returning the C_4F_8 flow back to a ramp of 50–25 SCCM. The etch yielded bar widths with a nonlinear taper. Specifically, the bar widths tapered from ≈120 to 90 nm along the first 500 nm of depth, and gradually tapered to 70 nm at the base. An improved etch was developed that kept the etch step constant at 1.2 s, and ramped the deposition step from 1.6 to 1.5 s. The improved etch yielded bar widths tapering approximately linearly from ≈100 nm at the top, to 80 nm at the base. See Fig. 10 for SEM images of the etch results.

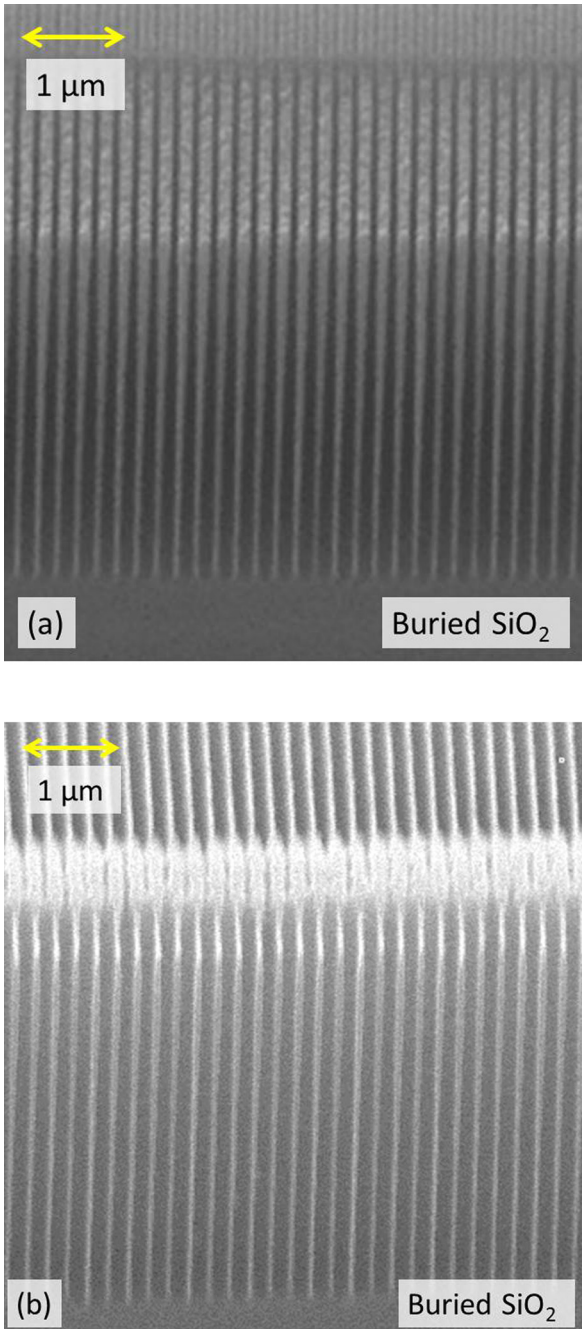

FIG. 8. (Color online) Preliminary nanoscale Bosch process result with tapered profile. (a) Cross section SEM imagery of 200 nm-pitch CAT grating etch stopping on buried SiO_2. Observe the tapered profile. The etch followed Table I except the C_4F_8 flow rate ramped from 25 to 0 SCCM. The duration was 220 loops. (b.) Cross section SEM imagery of 200 nm-pitch CAT grating from (a) after KOH polishing with 10% concentration for 30 s.

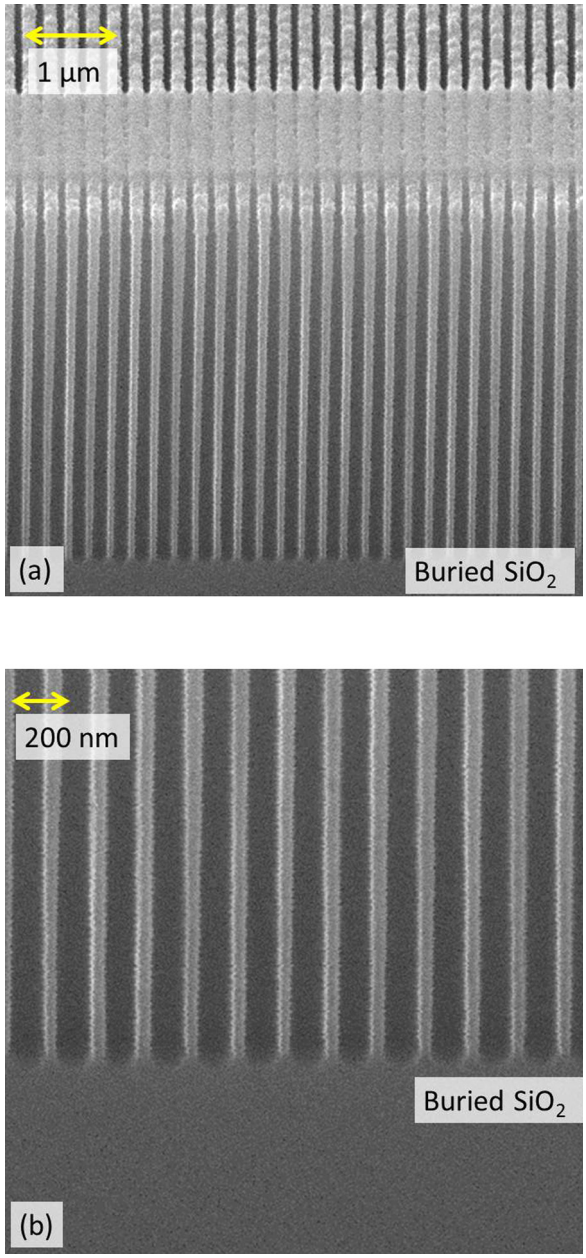

FIG. 9. (Color online) Improved nanoscale Bosch process result with tapered profile. (a) Cross section SEM imagery of 200 nm-pitch CAT grating DRIE. (b) Zoomed-in cross section SEM imagery of 200 nm-pitch CAT grating etch stopping on buried SiO_2. The etch followed Table I except the C_4F_8 flow rate ramped from 25 to 10 SCCM. The duration was 220 loops. "Wiggliness" in the lines is due to microscope vibrations.

The most notable drawback of the Bosch process is scallops in the sidewalls from the isotropic etch step. The depth of the scallops can typically range from 20 to 40 nm. Scallops were insignificant in all the experiments with nanoscale ultra-high aspect ratio etches. The duration of the etch and deposition steps is often how the scallops are controlled; however, 40 nm scallops were observed on low-aspect ratio features. Specifically, the aspect ratio was less than 1, and both DRIE steps were 1.2 s, the shortest times possible. The scallops on the high-aspect ratio etches were significantly less when using identical etch parameters. The scallops on the order of 20 nm were observed at the top of the grating bars and gradually reduced to below the resolution of the SEM at a depth of 500 nm. It is possible that the aspect ratio of the channel being etched creates a mask that filters only neutral fluorine atoms with low lateral motion. The $\arctan(w/d)$, where w is the width of the channel and d is the depth, determines the ratio of lateral to vertical velocity that a neutral particle can have, and make a direct impact on the sidewall at the bottom of a channel. This dramatically reduces the flux of particles to the

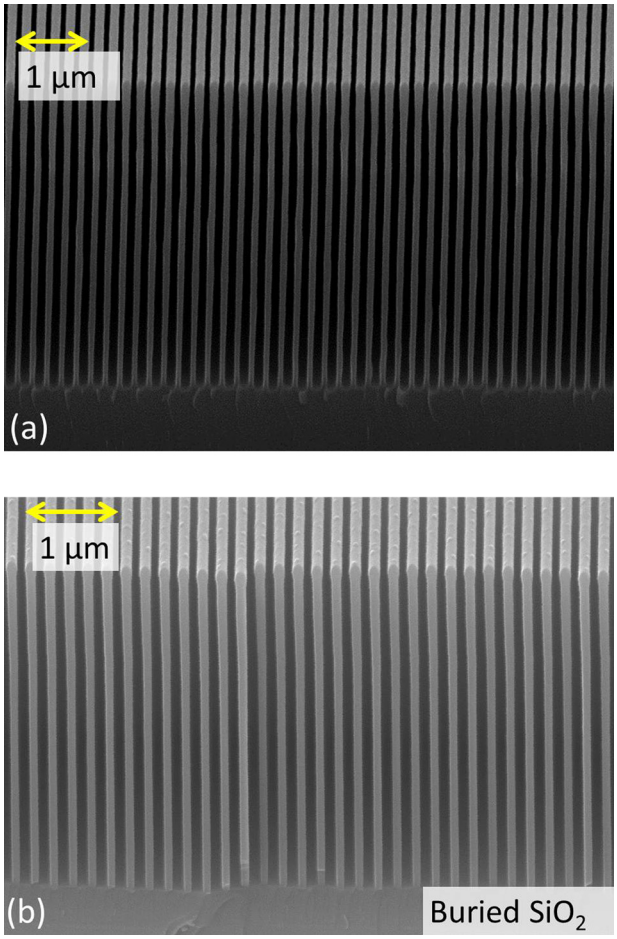

FIG. 10. (Color online) Nearly ideal nanoscale Bosch process results with shallow-tapered profiles. (a) Cross section SEM imagery of 200 nm-pitch CAT grating DRIE in bulk silicon. The etch followed Table I except the etch step increased with time from 1.2 to 1.5 s and the deposition step decreased from 1.5 to 1.2 s. The duration was 130 loops. (b) Cross section SEM imagery of 200 nm-pitch CAT grating etch stopping on buried SiO_2. The etch followed Table I except the etch step was constant at 1.2 s and the deposition step ramped from 1.6 to 1.5 s. The duration was 130 loops.

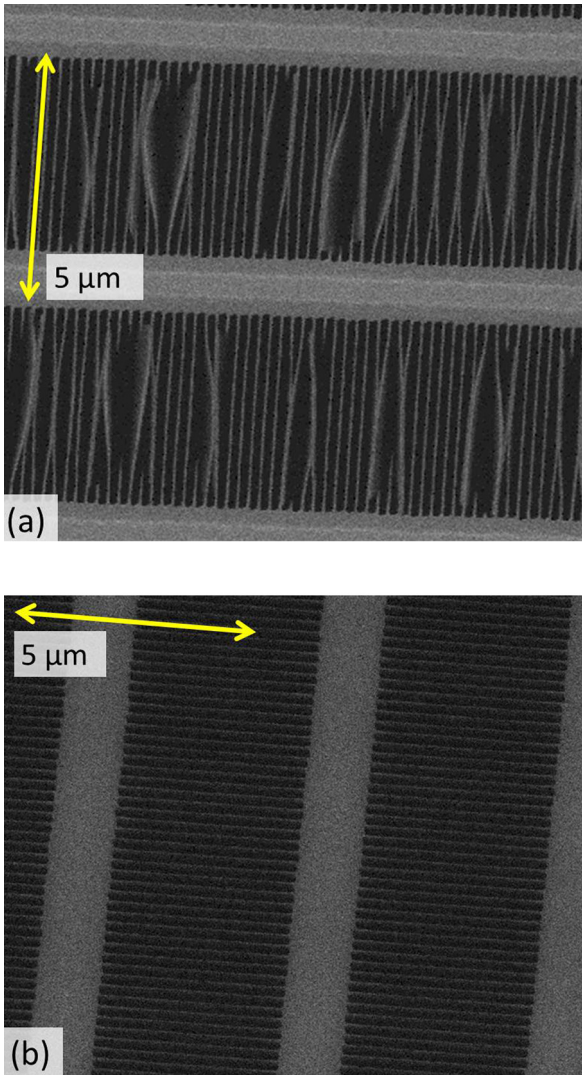

FIG. 11. (Color online) Bottom view SEM images of 200 nm-pitch freestanding CAT gratings comparing the old and new protective-coating processes. (a) Damaged lines from spinning the photoresist material after critical-point drying. (b) Undamaged lines from the new immersive filling process after critical-point drying. Note the bar thickness is under 50 nm, indicating a very gentle process.

sidewalls. The reduction in the overall etch rate of high aspect ratio structures is known as the lag effect, and has been discussed by Gottscho *et al*. and Volland *et al*.[27,28] Shadowing of reactants from the features is a major cause of this effect and likely reduces scalloping as well.

IV. FRONT-SIDE PROTECTIVE COATING

The CAT grating bars are fragile and a protective coating is critical for subsequent fabrication steps. After polishing with KOH, the grating is rinsed in DI water and transferred to roughly 200 ml denatured ethyl alcohol and then to acetone. The CAT grating bars are then filled with AZ Electronic Materials 4620 photoresist. The photoresist is poured from a bottle roughly 10 cm from the sample in acetone, and the stream of photoresist is kept about 1 cm away from the edge of the sample, so it would dissolve into the acetone. This process allowed the channels between the grating bars to be gradually filled with photoresist. Once the sample was clearly immersed in a solution of photoresist and acetone, the stream of photoresist was moved directly over the sample to coat it with a layer at approximately full viscosity. The sample was removed and spun at 1500 rpm for 60 s and baked at 90 °C for 60 s to create an even and solid protective coating.

This improved filling process was critical to achieving undamaged CAT gratings. The sample was critical-point dried after KOH polishing during the previous process. The protective coating of photoresist was then applied via a pipette and spin coated over the sample to fill the grating channels. This process worked well for grating bars thicker than 100 nm; however, it could crack and destroy thinner grating bars. See Fig. 11 for SEM images of CAT gratings fabricated with both methods. The new process enabled CAT gratings to be fabricated without any noticeable damage with bars under 50 nm-thick. The old method prevented CAT grating bars from being polished in the integrated process.

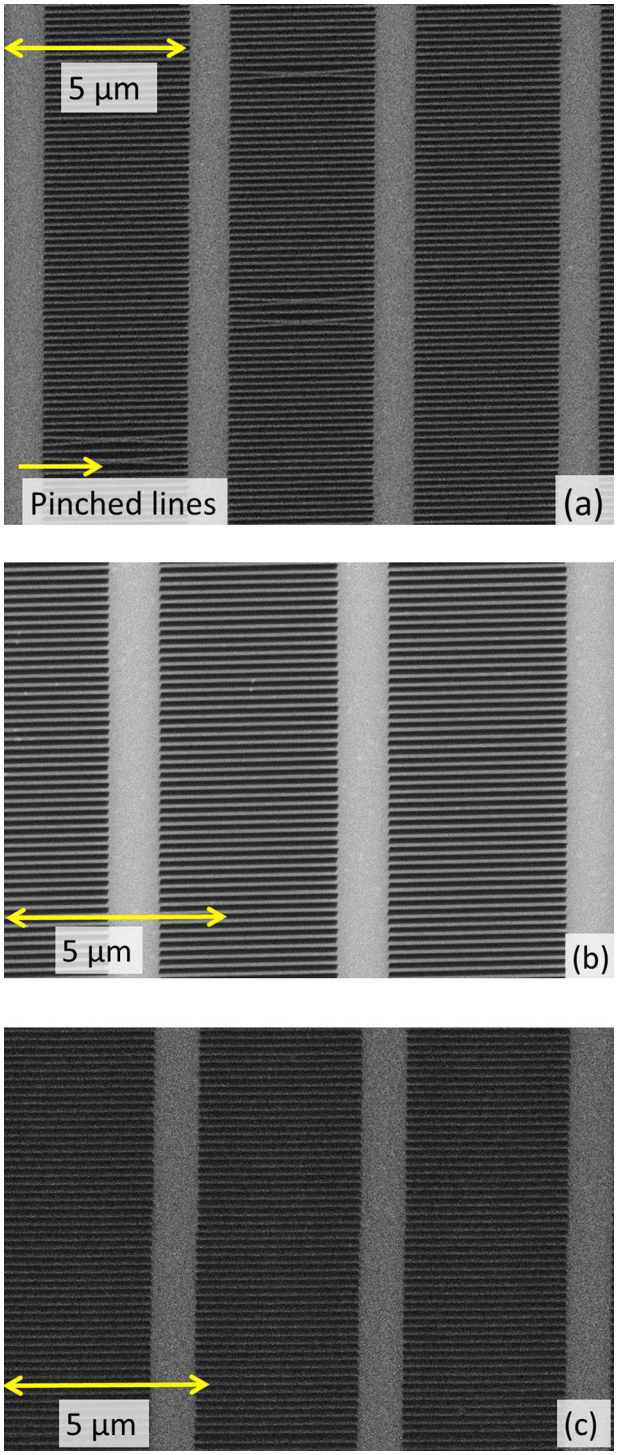

FIG. 12. (Color online) Comparison of vapor HF results before and after adjusting the sample and lamp distances. (a) Top view SEM image of a 200 nm-pitch freestanding CAT grating with CAT grating lines pinched from vapor HF step. (b) Top view SEM image of a 200 nm-pitch freestanding CAT grating with low duty-cycle lines. (c) Bottom view SEM image of a 200 nm-pitch freestanding CAT grating with low duty-cycle lines. Both (b) and (c) images show damage-free and low duty-cycle lines.

V. FINAL STRUCTURE AFTER VAPOR HF ETCH

The final step is the vapor HF process to remove the buried SiO_2. This step is delicate and it is possible for water vapor to condense on the grating bars, pinching them together when drying.[29] Early processing showed pinched grating lines after the vapor HF step, as shown in Fig. 12(a). The damage was not observed after the previous critical-point dry step, indicating the vapor HF was the cause. The vapor HF setup consisted of a Teflon beaker filled with approximately 25 ml of 49% HF with two Teflon bars spanning the top to hold the sample. A 75 W infrared bulb in a metal reflector approximately 200 mm in size was held about 3 cm from the sample to heat it. The distance from the HF reservoir to the sample was approximately 9 cm. The entire apparatus was placed in a fume hood set at room temperature. See Fig. 13 for a conceptual drawing of the vapor HF tool.

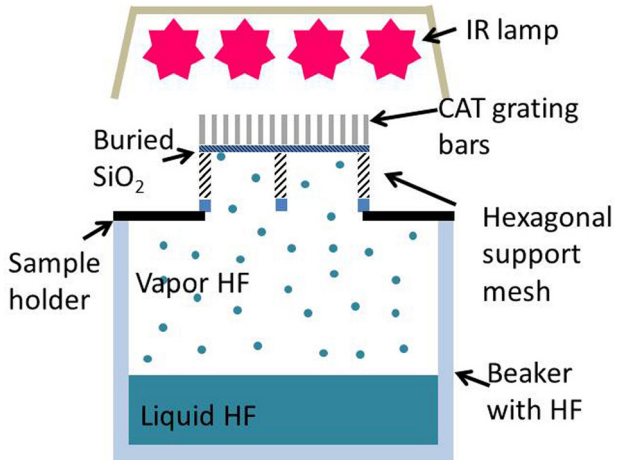

FIG. 13. (Color online) Conceptual drawing of vapor HF setup to etch buried SiO_2.

Prior experiments that yielded pinched lines had an 8 cm distance between the HF and the sample, and 5 cm between the bulb and sample. The etch is done for approximately 210 min, and the sample is regularly inspected throughout to prevent over-etching. The CAT grating bars and level 1 support structure are only attached to the level 2 hexagons by the buried SiO_2, which can be etched away releasing the grating. As a result, the etch must be carefully watched, and the sample removed once the buried SiO_2 is etched. The vapor HF step is still in development, and more work needs to be done to yield consistent results. Qualitatively, the distance between the lamp and the sample determines the temperature of the vapor and sample. The distance between the liquid HF and sample also affects the sample temperature and the local concentration of vapor HF.

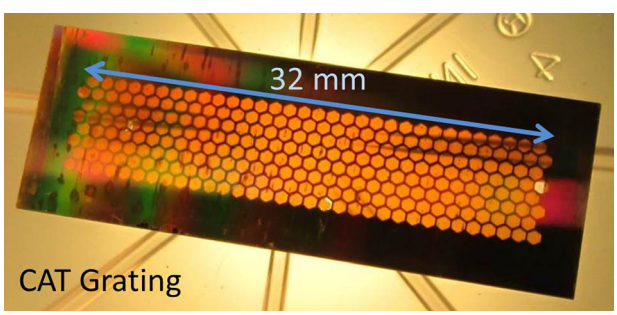

FIG. 14. (Color online) Photograph image of completed 200 nm-pitch freestanding CAT grating.

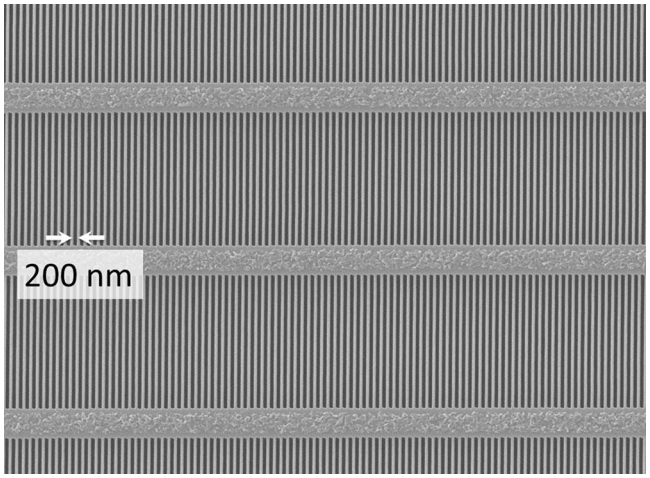

FIG. 15. Top view SEM imagery of a 200 nm-pitch freestanding CAT grating with nearly perfect lines.

Figure 12 shows top and bottom views of freestanding gratings without damage after the refined vapor HF process. See Fig. 14 for a photograph of an entire high quality grating. A few of the hexagon membranes have been damaged from handling mistakes. The gratings are processed manually, and their quality is improving as more steps are becoming routine. See Fig. 15 for a SEM image of a nearly perfect CAT grating that was used for tests demonstrating record-high resolving power.

VI. CONCLUSION

A fabrication process has been developed that integrates 200 nm-pitch ultrahigh aspect ratio DRIE with KOH polishing to create freestanding gratings. This process has produced gratings that are significantly more efficient and enable higher resolving power than any past soft x-ray transmission grating. An improved nanoscale DRIE step was presented to enable damage-free gratings after subsequent KOH polishing, backside processing, and numerous cleaning steps. A novel procedure was developed to fill the channels of the KOH-polished CAT grating bars, reducing damage compared to a previously developed filling procedure, which had been acceptable for unpolished lines. A gentle vapor HF step was developed to remove the buried SiO_2 at the end of the process. This process created over ten freestanding CAT gratings that were used for both efficiency and resolution tests.

ACKNOWLEDGMENTS

This work was funded by NASA Grant Nos. NNX15AC43G, NNX12AF21G, and NNX11AF30G, and the MIT Kavli Institute. Specific thanks to Martin Klingensmith of the MIT Space Nanotechnology Lab, James Daley of the MIT Nanostructures Lab, Vicky Diadiuk, Dennis Ward, Dave Terry, and Paul Tierney of the MIT Microsystems Technology Laboratories, Brian VanDerElzen of the University of Michigan Lurie Nanofabrication Facility and Frank di Piazza of Burkelynn Nano Solutions.

[1]A. Bruccoleri, P. Mukherjee, R. K. Heilmann, J. Yam, M. L. Schattenburg, and F. DiPiazza, J. Vac. Sci. Technol., B **30**, 06FF03 (2012).
[2]A. R. Bruccoleri, D. Guan, R. K. Heilmann, S. Vargo, F. DiPiazza, and M. L. Schattenburg, Proc. SPIE **8861**, 886119 (2013).
[3]R. K. Heilmann, A. R. Bruccoleri, D. Guan, and M. L. Schattenburg, Proc. SPIE **8861**, 886118 (2013).
[4]R. K. Heilmann, A. R. Bruccoleri, D. Guan, and M. L. Schattenburg, Proc. SPIE **9144**, 91441A (2014).
[5]R. K. Heilmann, A. R. Bruccoleri, and M. L. Schattenburg, Proc. SPIE **9603**, 960314 (2015).
[6]R. K. Heilmann *et al.*, Proc. SPIE **7732**, 77321J (2010).
[7]M. W. Bautz *et al.*, Proc. SPIE **8443**, 844315 (2012).
[8]D. W. Keith, M. L. Schattenburg, H. I. Smith, and D. E. Pritchard, Phys. Rev. Lett. **61**, 1580 (1988).
[9]J. T. M. van Beek, R. C. Fleming, P. S. Hindle, J. D. Prentiss, M. L. Schattenburg, and S. Ritzau, J. Vac. Sci. Technol., B **16**, 3911 (1998).
[10]C. David, J. Bruder, T. Rohbeck, C. Grunzweig, C. Kottler, A. Diaz, O. Bunk, and F. Pfeiffer, Microelectron. Eng. **84**, 1172 (2007).
[11]A. Bruccoleri, D. Guan, P. Mukherjee, R. K. Heilmann, M. L. Schattenburg, and S. Vargo, J. Vac. Sci. Technol., B **31**, 06FF02 (2013).
[12]J. A. Bookbinder, R. K. Smith, S. Bandler, M. Garcia, A. Hornschemeier, R. Petre, and A. Ptak, Proc. SPIE **8443**, 844317 (2012).
[13]A. Vikhlinin *et al.*, Proc. SPIE **8443**, 844316 (2012).
[14]R. K. Heilmann, M. Ahn, A. Bruccoleri, C.-H. Chang, E. M. Gullikson, P. Mukherjee, and M. L. Schattenburg, Appl. Opt. **50**, 1364 (2011).
[15]K. Flanagan *et al.*, Proc. SPIE **6688**, 66880Y (2007).
[16]C. R. Canizares *et al.*, Publ. Astron. Soc. Pac. **117**, 1144 (2005).
[17]R. K. Heilmann, M. Ahn, and M. L. Schattenburg, Proc. SPIE **7011**, 701106 (2008).
[18]C. R. Canizares, M. L. Schattenburg, and H. I. Smith, Proc. SPIE **597**, 253 (1986).
[19]F. Paerels, Space Sci. Rev. **157**, 15 (2010).
[20]R. K. Heilmann, A. Bruccoleri, J. Kolodziejczak, J. Gaskin, S. L. O'Dell, R. Bathia, and M. L. Schattenburg, Proc. SPIE **9905**, 99051X (2016).
[21]M. Ahn, R. K. Heilmann, and M. L. Schattenburg, J. Vac. Sci. Technol., B **26**, 2179 (2008).
[22]A. Bruccoleri, "Fabrication of high throughput critical-angle X-ray transmission gratings for wavelength-dispersive spectroscopy," Doctoral thesis (Department of Aeronautics and Astronautics, Massachusetts Institute of Technology, 2013).
[23]P. Mukherjee, A. Bruccoleri, R. K. Heilmann, M. L. Schattenburg, A. Kaplan, and L. Guo, J. Vac. Sci. Technol., B **28**, C6P70 (2010).
[24]I. W. Rangelow, J. Vac. Sci. Technol., A **21**, 1550 (2003).
[25]B. Wu, A. Kumar, and S. Pamarthy, J. Appl. Phys. **108**, 051101 (2010).
[26]M. M. Mirza, H. Zhou, P. Velha, X. Li, K. E. Docherty, A. Samarelli, G. Ternent, and D. J. Paul, J. Vac. Sci. Technol., B **30**, 06FF02 (2012).
[27]R. A. Gottscho, C. W. Jurgensen, and D. J. Vitkavage, J. Vac. Sci. Technol., B **10**, 2133 (1992).
[28]B. E. Volland, T. Ivanov, and I. W. Rangelow, J. Vac. Sci. Technol., B **20**, 3111 (2002).
[29]Y. Fukuta, H. Fujita, and H. Toshiyoshi, Jpn. J. Appl. Phys., Part 1 **42**, 3690 (2003).